Vibronic structure of the valence π-photoelectron bands in furan, pyrrole, and thiophene

A. B. Trofimov,[a] H. Köppel, and J. Schirmer
Theoretische Chemie, Physikalisch-Chemisches Institut, Universität Heidelberg, Im Neuenheimer Feld 253, D-69120 Heidelberg, Germany

(Received 13 February 1998; accepted 10 April 1998)

The $^2A_2$ and $^2B_1$ states formed in the ionization of the outermost π orbitals in furan, pyrrole and thiophene are shown to interact vibronically via nontotally symmetric b_2 vibrational modes. The interaction is strongest in pyrrole and thiophene, where the conical intersection between the two adiabatic surfaces occurs near the minimum of the upper ($^2B_1$) state. The resulting nonadiabatic effects manifest themselves in the $^2B_1$ bands by a lack of resolved structure in case of pyrrole and thiophene, and by a line broadening in case of furan. The spectra are investigated using a linear vibronic coupling model. All totally symmetric a_1 (tuning) modes and nontotally symmetric b_2 (coupling) modes describing the ring motion are taken into account. The parameters of the model are obtained with the aid of *ab initio* calculations. The ground state optimized geometries and vibrational frequencies are computed at the level of the second-order Møller–Plesset perturbation theory, while the dependence of the ionization energies on the nuclear configuration is evaluated using the outer valence Green's function method. Where appropriate, assignments of the observed structure are given. © *1998 American Institute of Physics.* [S0021-9606(98)02127-8]

I. INTRODUCTION

The five-membered heterocycles furan, pyrrole and thiophene play a prominent role in the current organic chemistry, molecular biology and material science. They serve as initial substances for many important syntheses, form the structural units of various natural products, and represent the building blocks for promising novel materials.[1] Hence, the physical chemistry, electronic structure, and spectroscopy of these molecules attract traditionally high attention.

At present, the ground-state characteristics of furan, pyrrole and thiophene are well established. All these molecules are five-membered ring species of C_{2v} symmetry (Fig. 1) in which the four p-electrons of the carbon atoms and a lone pair of the heteroatom form a stable six-electron aromatic system characterized by three doubly occupied π-molecular orbitals (MOs). One of these, $\pi_1(1b_1)$ ($2b_1$ in thiophene) is largely localized on the heteroatom and is relatively low in energy. The other two MOs, $\pi_2(2b_1)$ ($3b_1$ in thiophene) and $\pi_3(1a_2)$, are well delocalized; as the outermost occupied orbitals (Fig. 1) they determine, to a large extent, the chemical properties and the reactivity. The detachment of an electron from the π_1 and π_2 orbitals gives rise to the lowest two ionization bands in the photoelectron spectra, corresponding to cations in the $^2A_2$ and $^2B_1$ states. The energetic order of the corresponding vertical ionization potentials (IPs) is the same for all three molecules $\mathrm{IP}(^2B_1) > \mathrm{IP}(^2A_2)$, which has been confirmed by various experimental[2–7] and theoretical[8] studies.

The major source of experimental data on the valence-shell ionization of furan, pyrrole and thiophene are the high-resolution photoelectron spectra of Derrick *et al.*[4–7] These authors studied the vibrational structure of the $^2A_2(\pi_3^{-1})$ and $^2B_1(\pi_2^{-1})$ bands and succeeded in assigning many individual lines. For all three molecules, the $^2A_2(\pi_3^{-1})$ band exhibits a pronounced vibrational structure. The $^2A_2$ bands in furan and pyrrole are rather similar. A somewhat different, but also highly structured spectral envelope is observed in the case of thiophene. By contrast, the $^2B_1(\pi_2^{-1})$ bands are notably broader and, in the case of pyrrole and thiophene, show no resolved vibrational structure at all. No explanation for the latter fact has been given so far.

A theoretical effort to analyze the vibrational structure of the $^2A_2(\pi_3^{-1})$ and $^2B_1(\pi_2^{-1})$ photoelectron bands in furan, pyrrole and thiophene has been made by Takeshita *et al.*[9–11] These authors performed self-consistent field (SCF) calculations for the ground and ionized states and computed Franck–Condon (FC) factors for vibronic transitions using a shifted harmonic oscillator model. This approach allowed for a qualitatively correct description of the lower ($^2A_2$) bands but failed to reproduce the structure of the upper ($^2B_1$) bands. As is well known,[12] a broad, diffuse spectral band or an irregular vibrational structure are often the characteristic signatures of nonadiabatic effects. In the present case, a breakdown of the adiabatic approximation may be anticipated, since there is the possibility of linear vibronic coupling between the $^2A_2$ and $^2B_1$ states via a set of nontotally symmetric b_2 vibrational modes ($A_2 \otimes B_1 \otimes b_2 \supset A_1$). The failure of the theoretical approach of Takeshita *et al.* to reproduce the shape of the $^2B_1(\pi_2^{-1})$ band within the adiabatic approximation supports the above suggestion. For a more appropriate theoretical treatment of this situation it is necessary to go beyond the Born–Oppenheimer and Franck–Condon approximations. In this paper we report on the results of such a treatment of the nuclear dynamics[12] of the

[a]Author to whom correspondence should be addressed. Permanent address: Laboratory of Quantum Chemistry, Computer Center, Irkutsk State University, 664003 Irkutsk, Russian Federation.

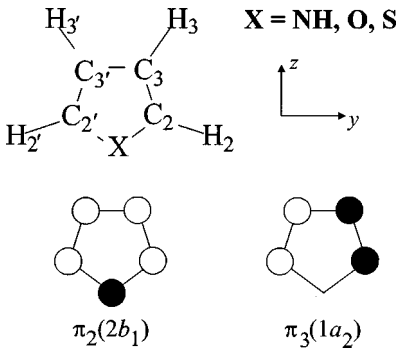

FIG. 1. Five-membered heterocycles furan (X=O), pyrrole (X=NH), thiophene (X=S) and their outermost occupied π orbitals.

π-electron ionization of furan, pyrrole and thiophene. In this approach, which has been successfully applied in the past to a number of vibronic coupling systems,[12] the nuclear dynamics of the valence-shell π-orbital ionization is described by a model Hamiltonian assuming *linear vibronic coupling* of the two *diabatic* electronic states, $^2A_2$ and $^2B_1$. In the present case there are 7 (8 in pyrrole) suitable b_2 (*coupling*) modes which have to be considered together with 8 (9 in pyrrole) a_1 (*tuning*) modes. The so-called *intrastate* and *interstate coupling constants* which are parameters of the model associated with a_1 and b_2 modes, respectively, are derived from *ab initio* calculations of the ionization energies. The latter step is performed using the outer valence Green's function (OVGF) method.[13] The ground-state vibrational frequencies entering the present vibronic coupling model are computed for the optimized ground-state equilibrium geometry at the level of second-order Møller–Plesset (MP2) perturbation theory.

II. THEORETICAL FRAMEWORK FOR TREATING THE NUCLEAR DYNAMICS

A. The linear vibronic coupling model

In the present work we study the vibronic structure of the $^2A_2(\pi_3^{-1})$ and $^2B_1(\pi_2^{-1})$ photoelectron bands within the framework of a general multimode two-state vibronic coupling model as described in Ref. 12. In this approach the central role is played by the concept of *diabatic* electronic states[14] which considerably simplifies the solution of the vibronic coupling problem. In the diabatic electronic representation, a final vibronic state is given in the form

$$\Psi_m(\mathbf{r};\mathbf{Q})=\Phi_1(\mathbf{r};\mathbf{Q})\chi_{1m}(\mathbf{Q})+\Phi_2(\mathbf{r};\mathbf{Q})\chi_{2m}(\mathbf{Q}), \quad (2.1)$$

where $\Phi_i(\mathbf{r};\mathbf{Q})$, $i=1, 2$, denote the diabatic electronic wave functions associated with the ionic states $^2A_2$ and $^2B_1$, respectively, under consideration; $\mathbf{r}$ and $\mathbf{Q}$ denote collectively the electronic and nuclear coordinates, respectively. The vibrational wave functions $\chi_{1m}(\mathbf{Q})$ and $\chi_{2m}(\mathbf{Q})$ in Eq. (2.1) are determined as the eigenfunction components of a two-dimensional vibrational Hamiltonian according to

$$\hat{\mathbf{H}}\begin{pmatrix}\chi_{1m}\\ \chi_{2m}\end{pmatrix}=e_m\begin{pmatrix}\chi_{1m}\\ \chi_{2m}\end{pmatrix}. \quad (2.2)$$

The Hamiltonian used in the present study is specified (in atomic units) as follows:

$$\hat{\mathbf{H}}=\hat{H}_0\mathbf{1}+\begin{pmatrix} E_1+\sqrt{2}\sum_{s\in g}\kappa_{1s}Q_s & \sqrt{2}\sum_{s\in u}\lambda_s Q_s \\ \sqrt{2}\sum_{s\in u}\lambda_s Q_s & E_2+\sqrt{2}\sum_{s\in g}\kappa_{2s}Q_s \end{pmatrix}. \quad (2.3)$$

In this expression $\mathbf{1}$ is a 2×2 unit matrix; E_i are the vertical ionization energies evaluated at the equilibrium geometry $\mathbf{Q_0}$ of the electronic ground state. The coefficients κ_{1s} and κ_{2s} are the *intrastate* coupling constants while λ_s are referred to as *interstate* coupling constants. The summations run over the sets of totally symmetric (g) and nontotally symmetric (u) normal modes, which in the present case comprise vibrations of a_1 and b_2 symmetry. The Q_s are dimensionless normal coordinates associated with the vibrational modes in the electronic ground state.[15,16] The vibrational Hamiltonian H_0 associated with the electronic ground state $|\Phi_0\rangle$,

$$\hat{H}_0=\frac{1}{2}\sum_{s\in g,u}\omega_s\left(-\frac{\partial^2}{\partial Q_s^2}+Q_s-1\right) \quad (2.4)$$

assumes noninteracting harmonic oscillators with frequencies ω_s, and the vibrational ground state energy is taken as the origin of the energy scale. Regarding the derivation of the present formalism, we note that in the diabatic electronic basis the coupling between the electronic states is introduced via the potential energy rather than via the kinetic energy of the nuclei. A Taylor expansion of the potential energy through linear terms in the nuclear coordinates yields the Hamiltonian [Eq. (2.3)] establishing the *linear vibronic coupling* (LVC) *model*. The quantities E_i, κ_{is}, λ_s and ω_s $(i=1, 2$ and $s\in g, u)$ represent parameters of the model and have to be determined in a suitable way.

Despite its simple appearance, the Hamiltonian [Eq. (2.3)] has proven successful in describing various complex photoelectron and photoabsorption spectra of small and medium-sized molecules.[17,12,18–20] Among the physical phenomena covered by the LVC model we mention first the possibility of symmetry lowering. If the repulsion of the two diabatic states [introduced by the off-diagonal element in the Hamiltonian (Eq. (2.3)] is sufficiently strong, the lower adiabatic potential energy surface (PES) will exhibit a symmetric double-minimum shape along the coordinates Q_s of the coupling modes, the minima being at $Q_s\neq 0$ for any of the coupling modes $(s\in u)$.[12] Second, the dependence of the lower adiabatic electronic wave function on the nuclear coordinates leads to the appearance of Franck–Condon forbidden lines in the low energy part of the spectrum via the mechanism of the vibronic intensity borrowing.[21,12] Finally, the strongest effects arise at higher energy as a result of (conical) intersections[22–24] of the two adiabatic PESs. Here the Born–Oppenheimer or adiabatic separation of the electronic and nuclear motion breaks down completely, leading to a complex, erratic line structure for energies above the minimum energy on the ''seam'' of conical intersections.[12] Under low resolution one will observe merely a diffuse spectral

envelope;[12,17–20] in a time-dependent description this is reflected by a femtosecond population decay of the upper electronic state.[25,26]

B. Calculation of the spectrum

The spectral function related to the photoelectron band is given by the golden rule expression

$$P(E)=\sum_m \sum_{i=1}^{2} |\langle \chi_{00}|\chi_{im}\rangle|^2 \delta(E-e_m) \tag{2.5}$$

where $|\chi_{00}\rangle$ is the vibrational part of the electronic and vibrational ground state.[12] A pedagogical derivation of Eq. (2.5) is given in the Appendix. Following Ref. 12 we use a variational ansatz to compute $|\chi_{im}\rangle$. To this end the Hamiltonian [Eq. (2.3)] is expanded in a direct-product basis $|n_1 \ldots n_M\rangle$ of harmonic oscillator eigenstates of H_0 [Eq. (2.4)]. Then $|\chi_{im}\rangle$ takes on the form

$$|\chi_{im}\rangle=\sum_{n_1 \ldots n_M} C_{im}^{n_1 \ldots n_M} |n_1 \ldots n_M\rangle, \tag{2.6}$$

where the summation is over all possible combinations of quantum numbers associated with the individual modes (M is the total number of modes in both sets g and u). In actual calculations we have to restrict the length of the expansion [Eq. (2.6)]. This is achieved by specifying the maximal level of excitation (in terms of quantum numbers n_s) for each mode v_s. A practically useful observation is that the Hamiltonian matrix decouples into two submatrices, associated with basis states of either A_2 and B_1 symmetry, which can be diagonalized separately.[12]

The standard Lanczos algorithm was used to generate the spectra.[27] Here the Lanczos algorithm is the method of choice as it can be implemented very efficiently to treat the highly sparse vibronic Hamiltonian matrix. Moreover, it provides rapid convergence of the spectral envelope. Typically, in the present calculations about 1000 Lanczos iteration steps yielded a well converged overall spectral profile. However, 10 000 iterations were needed in each case to obtain sufficiently converged individual lines. The spectral intensities are derived from the eigenvectors, which can easily be accomplished by choosing the ground-state harmonic oscillator function $|\chi_{00}\rangle \equiv |0 \ldots 0\rangle$ as the starting vector for the Lanczos iterations. The relative intensities are then given simply by the squared first components of the Lanczos eigenvectors.[12]

To study the effects of vibronic coupling it is useful to compare the results of the LVC model with the spectrum obtained in the approximation of uncoupled PES ($\lambda_s=0$). The spectrum then becomes the Poisson intensity distribution[12,28] defined for each of the electronic transitions $i(i=1,2)$,

$$P_i(E)=\sum_{n_1 \ldots n_g} |\langle 0 \ldots 0|n_1 \ldots n_g\rangle|^2 \times \delta\left(E-E_i+\sum_{s\in g} \omega_s(a_{is}-n_s)\right). \tag{2.7}$$

Here the Franck–Condon factors are given by

$$|\langle 0 \ldots 0|n_1 \ldots n_g\rangle|^2=\prod_{s\in g} \frac{(a_{is})^{n_s}}{n_s!} e^{-a_{is}}, \tag{2.8}$$

where $a_{is}=(\kappa_{is}/\omega_s)^2$ is the so-called Poisson (or vibrational strength) parameter. Comparison of the intensity distribution described by Eq. (2.7) with the results obtained in the vibronic coupling calculations gives useful insight into the role of vibronic coupling and in many cases simplifies the assignments of experimental spectra.

TABLE I. Calculated and experimental geometries of the five-membered heteroaromatic molecules (bond length in Å and angles in degrees).

	Furan (X=O)[a]		Pyrrole (X=N−H)[b]		Thiophene (X=S)[c]	
Parameter	MP2, this work	Expt.[d]	MP2, this work	Expt.[e]	MP2, this work	Expt.[f]
Bond length						
X—C_2	1.364	1.362	1.376	1.370	1.723	1.714
C_2—C_3	1.378	1.361	1.395	1.382	1.388	1.370
C_3—$C_{3'}$	1.436	1.430	1.427	1.417	1.427	1.423
C_2—H_2	1.088	1.075	1.089	1.076	1.091	1.078
C_3—H_3	1.089	1.077	1.090	1.077	1.093	1.081
X-H			1.013	0.996		
Angle						
$C_{2'}$—X—C_2	106.7	106.6	110.3	109.8	92.0	92.2
X—C_2—C_3	110.8	110.7	107.5	107.7	111.6	111.5
C_2—C_3—$C_{3'}$	105.9	106.1	107.4	107.4	112.4	112.5
X—C_2—H_2	115.8	116.0	121.2	121.5	120.3	119.9
C_2—C_3—H_3	126.3	127.8	125.6	125.5	123.1	123.2

[a]Total ground-state energy is −228.640545 hartree (SCF); −229.352231 hartree (MP2).
[b]Total ground-state energy is −208.826005 hartree (SCF); −209.525829 hartree (MP2).
[c]Total ground-state energy is −551.318442 hartree (SCF); −551.984070 hartree (MP2).
[d]Reference 31.
[e]Reference 32.
[f]Reference 33.

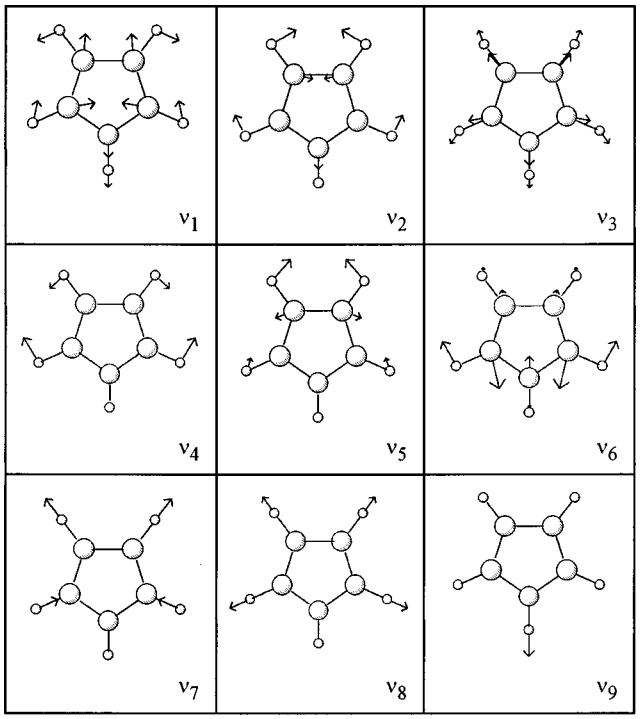

FIG. 2. Computed forms of the a_1 vibrational modes in the electronic ground state of five-membered heterocyclic molecules.

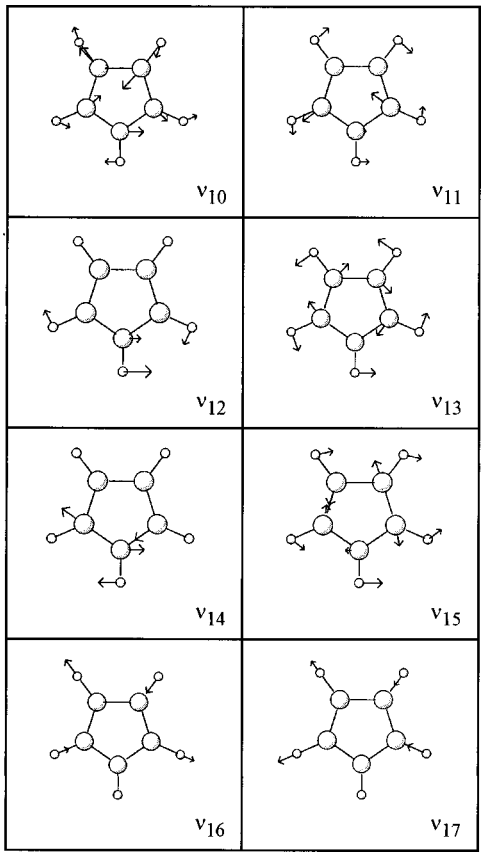

FIG. 3. Computed forms of the b_2 vibrational modes in the electronic ground state of five-membered heterocyclic molecules.

In the present work all spectral envelopes have been constructed from the line (or stick) spectra by convoluting them with Lorentzians of 0.015 eV FWHM (full width at half-maximum). The latter value is the estimated average experimental resolution in the spectra of Derrick *et al.*[4]

III. DETAILS OF THE *AB INITIO* CALCULATIONS

In the present work we pursue a consistent *ab initio* approach to parametrize our vibronic coupling model, which should ensure a comparable level of accuracy for all three molecules. The determination of the parameters is discussed in the following.

The ground-state energy calculations were carried out at the level of second-order Møller–Plesset perturbation theory. The outer-valence Green's function method[13] was used for the direct calculation of ionization energies. The correlation consistent valence polarized double-ζ (cc-pVDZ) Gaussian basis sets of Dunning[29] were used throughout. Both the MP2 and the OVGF methods allow for a qualitatively reliable description of the electronic structure (such as electron correlation and relaxation in the ionized states) at relatively small computational effort. The electronic structure calculations were performed using the GAUSSIAN program package.[30]

A. The ground-state parameters

In the initial step, the ground-state equilibrium geometries have been optimized. The results are listed in Table I. Also, some experimental data are shown for comparison. The ground-state energies associated with the optimal structures, calculated at the SCF and MP2 level are given in the footnotes of Table I. The theoretical and experimental[31–33] values of the geometrical parameters are seen to be in a good agreement, although the present results somewhat overestimate the bond lengths.

In the second step, the ground-state vibrational frequencies ω_s and the corresponding normal modes have been computed at the equilibrium geometries. Appropriate scaling yields the dimensionless normal coordinates Q_s required for the determination of the vibronic coupling constants. In the past various schemes have been used for labeling vibrations in the five-membered heterocyclic rings. In the present work we adopt for all three molecules the nomenclature of Lord and Miller[34] introduced for the case of pyrrole. The forms of the a_1 (labeled ν_1 through ν_9) and of the b_2 (labeled ν_{10} through ν_{17}) vibrations obtained in our calculations for pyrrole are shown in Figs. 2 and 3, respectively. Very similar vibrations result for furan and thiophene. Note that there are no modes ν_9 and ν_{12} (N-H stretching and bending, respectively) in the latter two molecules. The normal modes in Figs. 2 and 3 differ in some instances from the figures given by Lord and Miller, but they are in better agreement with the more recent results of Scott.[35,36] In Table II we compare the calculated harmonic frequencies of the a_1 and b_2 modes with available experimental data.[37–39] In general, rather satisfactory agreement between theory and experiment is observed for the frequencies of the skeleton vibrations ($\nu_1-\nu_6$, ν_{10}, ν_{11} and $\nu_{13}-\nu_{15}$).

TABLE II. Calculated and observed frequencies (cm^{-1}) of the a_1 and b_2 vibrations in the five-membered heteroaromatic molecules.

	Furan (X=O)		Pyrrole (X=N−H)		Thiophene (X=S)	
Mode	MP2, this work	Expt.[a]	MP2, this work	Expt.[b]	MP2, this work	Expt.[c]
a_1 modes						
ν_1	875	871	884	881	615	608
ν_2	1021	995	1041	1016	870	839
ν_3	1164	1066	1185	1144	1072	1036
ν_4	1116	1140	1103	1074	1088	1083
ν_5	1430	1384	1449	1382	1464	1409
ν_6	1520	1491	1520	1467	1399	1360
ν_7	3306	3140	3295	3129	3265	3098
ν_8	3332	3167	3317	3145	3293	3126
ν_9			3695	3531		
b_2 modes						
ν_{10}	878	873	862	865	769	751
ν_{11}	1059	1040	1061	1048	1093	1085
ν_{12}			1166	1134		
ν_{13}	1282	1267	1301	1287	1269	1256
ν_{14}	1249	1180	1510	1422	890	872
ν_{15}	1585	1556	1568	1530	1535	1507
ν_{16}	3295	3129	3284	3129	3251	3098
ν_{17}	3326	3161	3309	3145	3289	3125

[a]Reference 37.
[b]Reference 38.
[c]Reference 39.

B. Determination of coupling constants

The next step is the determination of the various coupling constants in the vibronic Hamiltonian. The intrastate coupling constants κ_{is} associated with the totally symmetric modes in Eq. (2.3) can be derived with the aid of the relation[12]

$$\kappa_{is}=\frac{1}{\sqrt{2}}\left(\frac{\partial V_i(\mathbf{Q})}{\partial Q_s}\right)_{\mathbf{Q_0}}, \quad s\in g \tag{3.1}$$

where $V_i(\mathbf{Q})$ denotes the adiabatic PES, $i=1$ and 2. Here the derivative with respect to the normal coordinate Q_s is to be taken at the equilibrium geometry of the electronic ground state. The interstate coupling constants λ_s in Eq. (2.3) can be obtained in a similar way according to

$$\lambda_s=\tfrac{1}{2}\,\mathbf{Q}_{1s}^{-1}\{[V_2(\mathbf{Q}_{1s})-V_1(\mathbf{Q}_{1s})]^2 - [V_2(\mathbf{Q}_0)-V_1(\mathbf{Q}_0)]^2\}^{1/2}, \quad s\in u, \tag{3.2}$$

where the nuclear configuration $\mathbf{Q}_{1s}$ has to be chosen along the coordinate Q_s in the vicinity of $\mathbf{Q}_0$. In practice, Eqs. (3.1) and (3.2) have been evaluated numerically, by computing the ionization energies at several nuclear configurations. The distorted configurations $\mathbf{Q}_{1s}=\mathbf{Q}_0\pm xQ_s$ have been constructed using the ground-state Cartesian normal coordinates Q_s and the scaling factor $x=0.5$.

The calculated intrastate coupling constants κ_{is} are given in Table III. These quantities indicate that there is an appreciable vibronic coupling via most of the skeleton vibrations $\nu_1-\nu_6$. As expected, a much weaker coupling effect is seen for the $\nu_7-\nu_9$ modes associated with the hydrogen motions. Similar observations apply for the interstate coupling constants λ_s in Table IV. These findings show that only the hydrogen stretching vibrations may be neglected in the vibronic calculations. As seen from Tables III and IV, the maximum quantum numbers of individual modes used for the generation of the harmonic oscillator basis range from 2 to 9. These values have been roughly optimized to minimize the size of the expansion but no thorough convergence tests have been performed. The resulting dimensions of the vibronic Hamiltonian matrices were 1 088 640, 5 225 472 and 7 962 624 in the case of furan, pyrrole, and thiophene, respectively.

The knowledge of the coupling constants κ_{is}, the vertical ionization energies and the ground-state vibrational frequencies allows one to calculate the adiabatic (0–0) ionization energies and the minimum energy of conical intersection of the two adiabatic surfaces. Since the explicit expressions for these quantities are quite lengthy, we show in Table V only the results of the calculations; for details the reader is referred to Ref. 12. Here the interesting finding is that in pyrrole and thiophene the intersection occurs very close to

TABLE III. Intrastate coupling constants κ_{is} (eV) and maximal quantum numbers n_s of a_1 vibrational modes in Eq. (2.6).

	Totally symmetric (a_1) vibrational modes								
	ν_1	ν_2	ν_3	ν_4	ν_5	ν_6	ν_7	ν_8	ν_9
Furan									
$\kappa_{is}(^2A_2)$	−0.035	0.034	−0.019	0.072	0.106	−0.129	0.003	−0.008	
$\kappa_{is}(^2B_1)$	0.072	−0.065	−0.080	−0.040	−0.069	−0.073	0.0	0.012	
n_s	4	3	3	3	4	5	0	0	
Pyrrole									
$\kappa_{is}(^2A_2)$	−0.049	0.032	−0.017	−0.074	0.128	−0.095	0.007	−0.001	−0.019
$\kappa_{is}(^2B_1)$	0.058	−0.062	−0.071	0.037	−0.093	−0.023	−0.003	0.012	−0.048
n_s	6	4	4	9	3	4	0	0	0
Thiophene									
$\kappa_{is}(^2A_2)$	−0.053	0.026	0.016	0.054	0.155	−0.077	0.008	−0.006	
$\kappa_{is}(^2B_1)$	0.042	−0.073	−0.067	−0.015	−0.071	0.027	0.004	−0.043	
n_s	9	6	4	2	2	8	0	0	

TABLE IV. Interstate coupling constants λ_s (eV) and maximal quantum numbers n_s of b_2 vibrational modes in Eq. (2.6).

		Nontotally symmetric (b_2) vibrational modes							
		ν_{10}	ν_{11}	ν_{12}	ν_{13}	ν_{14}	ν_{15}	ν_{16}	ν_{17}
Furan	λ_s	0.054	0.0		0.054	0.127	0.144	0.054	0.038
	n_s	4	0		3	7	6	0	0
Pyrrole	λ_s	0.050	0.0	0.064	0.0	0.129	0.111	0.041	0.0
	n_s	4	0	3	0	7	6	0	0
Thiophene	λ_s	0.085	0.046		0.046	0.054	0.104	0.029	0.021
	n_s	8	2		2	6	6	0	0

the adiabatic minimum of the upper state (0.04 and 0.01 eV, respectively). Hence, pronounced nonadiabatic effects in the spectra can be expected. By contrast, in furan such effects should be less important as here the intersection point is located 0.51 eV above the minimum of the upper state.

C. Vertical ionization energies

Let us recall that the vertical transition energies are primarily a theoretical notion that cannot directly be taken from experiment. Often, however, the center of gravity of an electronic band is a good approximation to the vertical transition energy. In principle, the $^2A_2(\pi_3^{-1})$ and $^2B_1(\pi_2^{-1})$ ionization energies in furan, pyrrole and thiophene are well established experimentally[2–7] and theoretically.[8–11] It should be noted that there has been some confusion concerning the experimental ''vertical'' ionization energies E_ν^{expt} used in the literature, as the values given by Derrick *et al.*[5–7] are identical to the energies of the adiabatic transitions E_{0-0}^{expt} for the $^2A_2$ band in all three molecules and for the $^2B_1$ band in furan (Table V). This is clearly incorrect, since the respective bands have widths of more than 0.4 eV and exhibit substantial spectral strength above the 0–0 transition. Using our theoretical data presented in Table V we can estimate the ''true'' experimental vertical ionization energies E_ν^{est}. To this end, we first evaluate the ''adiabatic lowering'' Δ_{ad}, that is, the difference between the calculated vertical and adiabatic energies. As seen from the Table V, the Δ_{ad} values vary between 0.14 and 0.22 eV. The deviation of the E_{0-0}^{th} from the experimental values (excepting $^2B_1$ bands in pyrrole and thiophene where the 0–0 lines cannot be resolved) is rather uniform and varies between 0.45 and 0.51 eV. We obtain very similar deviations by comparing our vertical energies with the positions of the $^2B_1$ band maxima in pyrrole and thiophene (0.47 and 0.45 eV, respectively). These observations confirm that the calculated Δ_{ad} values are quite realistic and indicate that the average absolute accuracy of our results for ionization energies is about 0.47 eV. By adding Δ_{ad} to E_{0-0}^{th}, we finally obtain the required estimates E_ν^{est} of the experimental vertical transition energies (Table V).

Before presenting the results of our dynamic calculations we repeat that purely *ab initio* data have been used for the parameters of the LVC model, including the vertical ionization energies E_ν^{th} from Table V.

TABLE V. Experimental and present theoretical vertical (v) and adiabatic (0–0) ionization energies; adiabatic energy lowering (Δ_{ad}) and estimated vertical ionization energies (E_v^{est}); minimum energy of conical intersection (E_{int}) and its position above the adiabatic minima of the electronic states (Δ_{int}).[a]

Molecule and state	Experiment[b]		Theory, this work					
	E_v^{expt}	E_{0-0}^{expt}	E_v^{th}	E_{0-0}^{th}	Δ_{ad}	E_v^{est}	E_{int}	Δ_{int}[f]
Furan							10.37	
$^2A_2$	8.88	8.88	8.58	8.37	0.21	9.09		2.00
$^2B_1$	10.31	10.31	10.05	9.85	0.20	10.51		0.51
Pyrrole							8.60	
$^2A_2$	8.21	8.21	7.91	7.69	0.22	8.43		0.91
$^2B_1$	9.20[c]	9.20[d]	8.73	8.57	0.16	9.20[e]		0.04
Thiophene							8.93	
$^2A_2$	8.87	8.87	8.65	8.42	0.23	9.10		0.51
$^2B_1$	9.52[c]	~9.3[d]	9.07	8.93	0.14	9.52[e]		0.01

[a]All quantities are in eV.
[b]Reference 5 (furan); Ref. 6 (pyrrole); Ref. 7 (thiophene).
[c]Band maxima.
[d]Experimental situation is uncertain.
[e]Taken as the experimental band maximum.
[f]Calculated using E_{0-0}^{th} and E_{int} with three decimal digits; the results are rounded to two decimal digits.

TABLE VI. Theoretical and experimental assignment of the vibrational structure of the $^2A_2(\pi_3^{-1})$ photoelectron band in furan.[a]

Experiment[b]				Poisson distribution, this work			Theory[c]		
Feature[d]	Assign.	Energy	Intens.	Assign.	Energy	Intens.[e]	Assign.[f]	Energy	Intens.
A	0	0	vs	0	0	0.27	0	0	s
γ		500	w						
δ		799	w	υ_{10}	807[g]	0.002[g]			
B	υ_1	839	m	υ_1	875	0.03	υ_1	953	m
C	υ_4	1073	s	υ_2	1021	0.02	υ_3	1146	w
				υ_4	1116	0.07	υ_4	1187	s
D	υ_6	1420	s	υ_5	1430	0.10	υ_5	1578	s
				υ_6	1520	0.13			
ϵ		1565	w	$2\upsilon_{10}$	1613[g]	0.006[g]			
ξ		1742	w	A_1	1855[g]	0.005[g]			
E	$\upsilon_1+\upsilon_4$	1994	w	$\upsilon_1+\upsilon_4$	1991	0.01	$\upsilon_1+\upsilon_4$	2140	w
F	$2\upsilon_4$	2194	m	$\upsilon_2+\upsilon_4$	2137	0.01			
	$\upsilon_1+\upsilon_6$			$2\upsilon_4$	2232	0.01	$2\upsilon_4$	2374	w
				$\upsilon_1+\upsilon_5$	2305	0.01	$\upsilon_1+\upsilon_5$	2531	w
				$\upsilon_1+\upsilon_6$	2395	0.01			
G	$\upsilon_4+\upsilon_6$	2500	m	$\upsilon_2+\upsilon_5$	2451	0.01			
				$\upsilon_2+\upsilon_6$	2541	0.01	$\upsilon_3+\upsilon_5$	2724	w
				$\upsilon_4+\upsilon_5$	2546	0.03	$\upsilon_4+\upsilon_5$	2765	m
				$\upsilon_4+\upsilon_6$	2636	0.03			
H	$2\upsilon_6$	2823	m	$2\upsilon_5$	2860	0.02	$2\upsilon_5$	3156	m
				$\upsilon_5+\upsilon_6$	2950	0.05			
				$2\upsilon_6$	3040	0.03			

[a]The energies of transitions relative to the 0−0 origin (cm^{-1}). The spectral intensities are given by FC factors (present work), or characterized qualitatively as very strong (vs), strong (s), medium (m) and weak (w) (otherwise).
[b]References 4 and 5. The data for the spectral features designated with Greek letters derived in the present work.
[c]Reference 9.
[d]See Fig. 4.
[e]Only the transitions with intensities greater than 0.01 are shown.
[f]The final-state vibrational modes. The modes υ_3, and υ_4 and υ_5 have different character in the initial and the final electronic states.
[g]Calculations using vibronic coupling model.

IV. RESULTS AND DISCUSSION

A. Furan

1. The $^2A_2$ band

The experimental $^2A_2(\pi_3^{-1})$ photoelectron band of furan is shown in Fig. 4(A). In this spectrum Derrick *et al.*[4,5] have identified eight vibrationally excited levels which we have labeled by Latin letters A through H. In addition to these features we further distinguish several less prominent structures, not assigned previously. These are the maxima γ and ζ and the shoulders δ and ϵ.

The Poisson intensity distribution computed here [Fig. 4(C)] reproduces quite well the major features of the experimental spectrum in the $^2A_2$ band at lower energy.[40] The calculated transition energies (Table VI) are also in fair agreement with the experimental data of Derrick *et al.*[4,5] The transition frequencies given by Takeshita *et al.*[9,41] agree lees favorably with experiment,[4,5] probably because of the neglect of electronic correlation. For convenience of comparison in Table VI and in the following, the notations of the a_1 modes of Takeshita *et al.*[9–11] were converted to those of Lord and Miller.[34] Our results generally support the assignments of Derrick *et al.* and agree at lower energies also with those of Takeshita *et al.* As noted already by Takeshita *et al.*, the modes ν_2 and ν_5 play an important role in the $^2A_2$ ionization of furan together with the modes ν_1, ν_4 and ν_6, previously identified by Derrick *et al.* For example, peaks *C* and *D* do not correspond to single excitations as suggested by Derrick *et al.*, but rather result from the excitation of vibrations with similar frequencies, $(2_0^1,4_0^1)$ and $(5_0^1,6_0^1)$, respectively. The features $(\gamma-\zeta)$ cannot be explained by the Poisson distribution.

The success of the simple Poisson intensity distribution model in the explanation of the observed spectral envelope indicates that the final-state frequencies do not differ much from those in the electronic ground state. The latter fact has been experimentally established by Derrick *et al.*,[4] who attributed the similarity of vibrational frequencies in the π_2^{-1} and π_3^{-1} ionized and in the ground electronic states the strong delocalization of the π electrons in the aromatic systems. Thus, the vibrational structure of the final states, in the absence of pronounced vibronic coupling effects, can be assigned in terms of the ground-state vibrational modes, to a good approximation.

The consideration of vibronic interaction with the $^2B_1$ state does not modify the Poisson envelope very much. In the

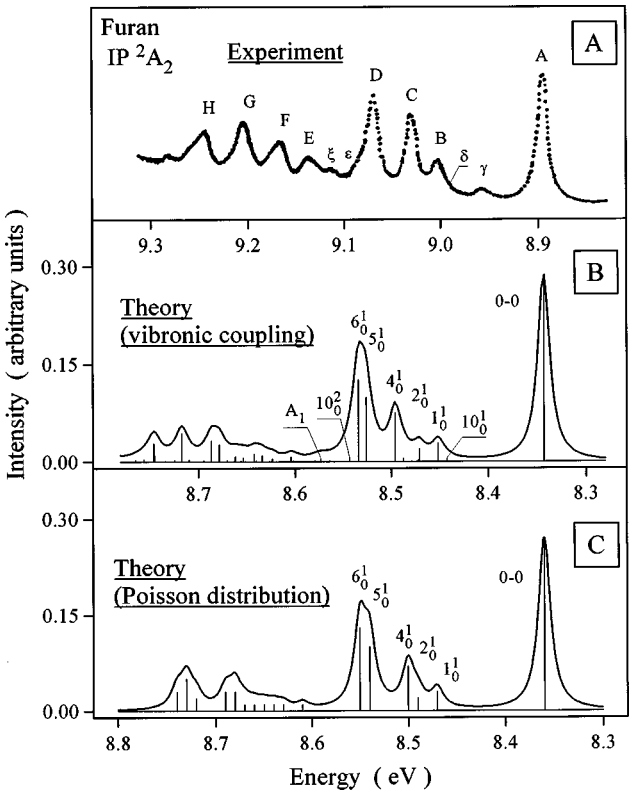

FIG. 4. Theoretical and experimental spectral envelopes of the $^2A_2(\pi_3^{-1})$ photoelectron band in furan.

vibronic spectrum [Fig. 4(B)] the relative positions of certain lines are slightly modified and few new lines of much smaller intensity can be seen. The picture of the two separate adiabatic energy surfaces holds here to a good approximation (see the discussion in Sec. IV D), and the additional lines can be regarded as being due to the nontotally symmetric modes via intensity borrowing. Almost certainly,[42] the very first of these lines corresponds to the excitation of a single quantum of the coupling mode ν_{10} with a modified frequency of 0.1 eV (807 cm^{-1}), which is in agreement with the final-state frequency of 0.105 eV (847 cm^{-1}) as estimated from the expression[43]

$$\omega_s' \approx \sqrt{\omega_s\left(\omega_s - \frac{4\lambda_s^2}{E_2 - E_1}\right)}. \tag{4.1}$$

The interpretation of intensity borrowing lines at higher energy is less obvious and we do not pursue this here. The presence of nontotally symmetric vibrations in the spectrum allows us to explain some of the features not addressed in the work of Derrick *et al.* The excitation 10_0^1, for example, gives rise to the shoulder δ at about 8.99 eV. As seen from the Table VI, its calculated and measured frequencies relative to the 0–0 origin (807 and 799 cm^{-1}, respectively) agree well. The shoulder ϵ near 9.09 eV (1565 cm^{-1} with respect to the 0–0 origin) is identified as a satellite line with calculated frequency of 1613 cm^{-1}. This feature could be assigned to the 10_0^2 transition by noticing that its frequency is just twice the frequency of the 10_0^1 line, and that the vibrational final state according to our calculations has A_1 symmetry. The weak maximum ζ at 9.12 eV (1742 cm^{-1} with respect to the 0–0 origin) correlates with the group of lines in the 8.55–8.58 eV region. The strongest of these lines has a calculated frequency of 1855 cm^{-1} and A_1 vibrational symmetry.

2. The $^2B_1$ band

For the $^2B_1(\pi_2^{-1})$ photoelectron band [Fig. 5(C)] the Poisson intensity distribution agrees less favorably with the experimental profile [Fig. 5(A)] than in the case of the $^2A_2(\pi_3^{-1})$ band. The theoretical spectrum predicts more structure than seen in the experiment. Also, the experimental spectrum is characterized here by notably broader lines. Some assignments, however, are possible. As seen from Table VII, our calculations predict high activity of the modes $\nu_1-\nu_6$, while again only the modes ν_1, ν_3 and ν_5 have been taken into consideration by Derrick *et al.*[4,5] Accordingly, some of the previous assignments have to be modified. For example, three transitions 2_0^1, 3_0^1 and 4_0^1 contribute to the shoulder C, whereas only one (3_0^1) has been identified by Derrick *et al.* Moreover, our calculations explain the maximum D as arising from two transitions, 5_0^1 and 6_0^1, from which only the former has been considered by Derrick *et al.* The results of Takeshita *et al.*[9] are in qualitative agreement with the present findings (Table VII). A major discrepancy from our results is that the modes ν_4 and ν_5 are found to be not active. In comparison with experiment, the transition energies calculated by Takeshita *et al.* seem to be systematically too large.

There is a notable increase of the linewidths in the $^2B_1(\pi_2^{-1})$ band, as compared to the case of the $^2A_2(\pi_3^{-1})$ band. This effect can be understood by inspecting results of the vibronic calculation. The spectrum in Fig. 5(B) largely reproduces the Poisson profile. However, the spectral peaks no longer correspond to individual lines, but rather arise from bunches of closely lying lines where the intensity is rapidly decreasing with the distance from the central line. By their shape and nature these structures resemble resonances. Indeed, they can be viewed as a result of weak interaction between the a_1 vibrations of the upper ($^2B_1$) adiabatic surface and a dense manifold of highly excited b_2 vibrational levels of the lower ($^2A_2$) surface. Since the overall shape of the spectrum is largely preserved and the position of the ''resonances'' are only slightly shifted with respect to the positions of the parent lines in the Poisson intensity distribution, the above assignment of the experimental spectrum (Table VII) can be expected to be realistic. The weak maximum γ seen in the experimental spectrum between peaks *A* and *B* cannot be explained by the present calculations.

B. Pyrrole

1. The $^2A_2$ band

The shape of the $^2A_2(\pi_3^{-1})$ photoelectron band in pyrrole [Fig. 6(A)] is quite similar to the one observed in furan. Derrick *et al.*[4,6] have identified and interpreted a number of transitions (labeled *A* through *K*) in terms of excitations of the four vibrational modes ν_1, ν_4, ν_5 and ν_6. Our Poisson analysis [Fig. 6(C)] predicts that in addition to the latter vibrations also ν_2 mode should play a role in the spectrum. The theoretical profile agrees well with experiment so that

TABLE VII. Theoretical and experimental assignment of the vibrational structure of the $^2B_1(\pi_2^{-1})$ photoelectron band in furan.[a]

Experiment[b]				Poisson distribution, this work			Theory[c]		
Feature[d]	Assign.	Energy	Intens.	Assign.	Energy	Intens.[e]	Assign.[f]	Energy	Intens.
A	0	0	vs	0	0	0.25	0	0	s
γ		403	w						
B	ν_1	871	s	ν_1	875	0.11	ν_1	935	s
C	ν_3	952	m	ν_2	1021	0.07	ν_2	1026	m
				ν_4	1116	0.02			
				ν_3	1164	0.08	ν_3	1222	w
D	ν_5	1355	w	ν_5	1430	0.04			
				ν_6	1520	0.04	ν_6	1589	m
E	$2\nu_1$	1855	m	$2\nu_1$	1750	0.02	$2\nu_1$	1870	m
	$2\nu_3$			$\nu_1+\nu_2$	1896	0.03			
	$\nu_1+\nu_3$			$\nu_1+\nu_4$	1991	0.01			
				$\nu_1+\nu_3$	2039	0.03	$\nu_1+\mu_3$	1961	m
				$2\nu_2$	2042	0.01	$2\nu_3$	2052	w
				$\nu_2+\nu_4$	2137	0.01			
				$\nu_2+\nu_3$	2185	0.02			

[a]See footnote a of Table VI.
[b]See footnote b of Table VI.
[c]See footnote c of Table VI.
[d]See Fig. 5.
[e]See footnote e of Table VI.
[f]The final-state vibrational modes.

the features ($A-E$) can be unambiguously assigned. In Table VIII we present our Poisson results in comparison with the data of Derrick *et al.*[4,6] and Takeshita *et al.*[10] Our assignments are consistent with those given by Derrick *et al.*, extending them in a few cases. For example, the peak *C*, which has been assigned to the 4_0^1 transition by Derrick *et al.*, is a combination of two transitions 2_0^1 and 4_0^1 according to our results. Similar situations are found at higher energy, where in several combination bands the mode ν_2 has been ignored by Derrick *et al.* The assignments made by Takeshita *et al.* are quite similar to ours. However, it should be noted that in the latter work the modes ν_3, ν_5 and ν_6 do not strictly correspond to those in the electronic ground state.

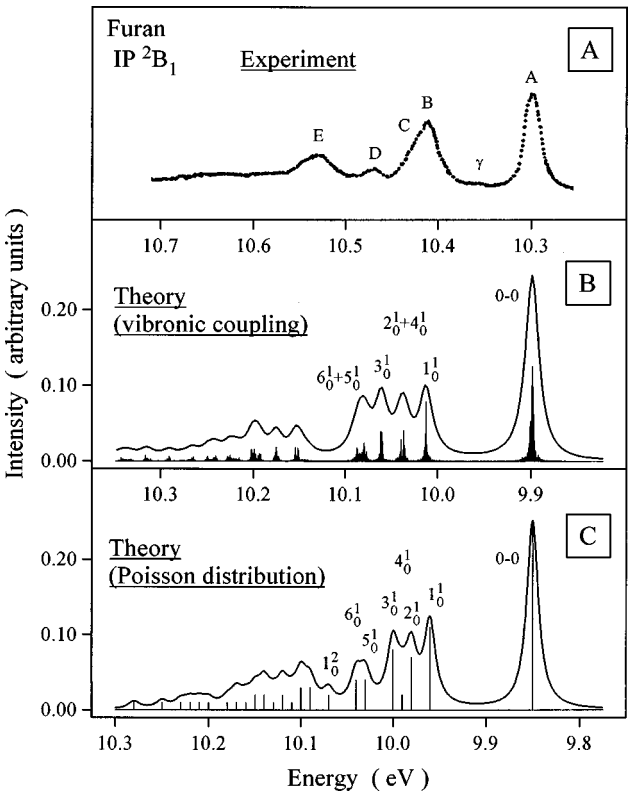

FIG. 5. Theoretical and experimental spectral envelopes of the $^2B_1(\pi_2^{-1})$ photoelectron band in furan.

The full vibronic spectrum in Fig. 6(B) resembles the spectral profile of the Poisson intensity distribution. However, at the level of individual lines some new features can be noticed. Whereas the transitions 1_0^1, 2_0^1 and 4_0^1 are only slightly affected, the location of the 5_0^1 and 6_0^1 lines in the vibronic spectrum is no longer obvious as here the spectrum is notably modified. The excitations 5_0^1 and 6_0^1 can probably be found near 7.85–7.90 eV, although the group of lines in this region may have a more complex origin. Many intensity-borrowing satellites are observed in the vibronic spectrum. Analogous to the case of furan, the lowest of these lines is located about 0.096 eV (774 cm^{-1}) above the 0–0 line and represents the 10_0^1 transition. The frequency of this transition estimated using Eq. (4.1) is 0.101 eV (815 cm^{-1}). The 10_0^1 transition correlates with the previously unidentified shoulder δ found about 0.086 eV (694 cm^{-1}) above the 0–0 line in the experimental spectrum.

2. The $^2B_1$ band

The $^2B_1(\pi_2^{-1})$ photoelectron band in pyrrole [Fig. 7(A)] differs strikingly from those considered above. All features are very broad and almost no structure can be discerned. The two prominent maxima *A* and *B* have been assigned by Der-

TABLE VIII. Theoretical and experimental assignment of the vibrational structure of the $^2A_2(\pi_3^{-1})$ photoelectron band in pyrrole.[a]

Experiment[b]				Poisson distribution, this work			Theory[c]		
Feature[d]	Assign.	Energy	Intens.	Assign.	Energy	Intens.[e]	Assign.[f]	Energy	Intens.
A	0	0	vs	0	0	0.26	0	0	s
γ		444	w						
δ		694	w	ν_{10}	774[g]	0.005[g]			
B	ν_1	871	m	ν_1	884	0.05	ν_1	956	m
C	ν_4	1065	s	ν_2	1041	0.02	ν_3	1146	s
				ν_4	1103	0.08	ν_4	1166	s
D	ν_5	1371	m	ν_5	1449	0.13	ν_5	1581	s
E	ν_6	1468	m	ν_6	1520	0.07	ν_6	1689	w
F	$2\nu_1$	1742	w	$2\nu_1$	1768	0.01	$2\nu_1$	1912	w
G	$\nu_1+\nu_4$	1936	mw	$\nu_1+\nu_4$	1987	0.02	$\nu_1+\nu_3$	2102	m
H	$2\nu_4$	2129	mw	$2\nu_4$	2206	0.01	$\nu_1+\nu_4$	2122	w
				$\nu_1+\nu_5$	2333	0.03	$2\nu_4$	2292	w
				$\nu_1+\nu_6$	2404	0.01	$\nu_3+\nu_4$	2312	w
I	$\nu_4+\nu_5$	2460	w	$\nu_2+\nu_5$	2490	0.01	$\nu_1+\nu_5$	2537	m
				$\nu_4+\nu_5$	2552	0.04	$\nu_3+\nu_7$	2727	m
J	$\nu_4+\nu_6$	2541	w	$\nu_4+\nu_6$	2623	0.02	$\nu_4+\nu_5$	2747	m
K	$\nu_5+\nu_6$	2839	w	$2\nu_5$	2898	0.03			
				$\nu_5+\nu_6$	2969	0.03	$2\nu_5$	3162	m
				$2\nu_6$	3040	0.01			

[a]See footnote a of Table VI.
[b]References 4 and 6. The data for the spectral features designated with Greek letters derived in the present work.
[c]Reference 10.
[d]See Fig. 6.
[e]See footnote e of Table VI.
[f]The final-state vibrational modes. The modes ν_3, ν_5 and ν_6 have different character in the initial and the final electronic states.
[g]See footnote g of Table VI.

rick *et al.*[4,6] to the 0–0 and 1_0^1 transitions, respectively. In view of the high experimental resolution the diffuse character of this band poses a puzzle that has not been addressed in the literature hitherto.

The Poisson intensity distribution plotted with the usual linewidth of 0.015 eV [Fig. 7(C)] differs markedly from the experimental profile. However, the agreement between the theoretical and experimental spectral profile could be improved by using a larger linewidth in the theoretical spectrum. Indeed, then the 0–0 line in the Poisson distribution would match the peak *A*, whereas the group of lines at higher energy beginning with the transition 1_0^1 would give rise to a broad maximum correlating with the maximum *B*. Our Poisson analysis predicts the modes $\nu_1-\nu_5$ to be active in the $^2B_1(\pi_2^{-1})$ ionization, which differs from the findings of Takeshita *et al.*[10] indicating an activity of ν_1, ν_4 and ν_5 modes. Unfortunately, Takeshita *et al.* do not compare their results to the high-quality spectrum of Derrick *et al.*,[4] but rather to the low-resolution spectrum of Turner *et al.*,[2] which they find to be in good agreement with their results. The question ''what makes the $^2B_1(\pi_2^{-1})$ photoelectron band in pyrrole so broad?'' is neither explained by the calculations of Takeshita *et al.*, nor by the present Poisson analysis.

The answer to this question is given by vibronic calculations. As seen in the spectrum in Fig. 7(B), vibronic interaction of the $^2B_1$ and the $^2A_2$ state leads to a completely different spectral profile than that of the Poisson distribution. Now the theoretical spectrum is in excellent qualitative agreement with experiment. The distinct spectral line structure seen in the Fig. 7(C) has turned into a complicated and irregular line pattern. The density of states is so high that any individual assignment of vibrational lines is impossible. However, it is probably legitimate to assume that the fairly distinct groups of transitions in vibronic spectrum near 8.7 and 8.85 eV are related to the transitions 0–0 through 5_0^1. Qualitatively this relationship can be understood as a redistribution of the spectral intensity of the a_1 transitions associated with the upper electronic state by mixing with a large number of excitations of b_2 modes associated with the lower electronic state.[12] This situation is similar to ''resonances'' observed for the $^2B_1(\pi_2^{-1})$ band in furan, but here much more pronounced due to the distinctly stronger vibronic interaction.

C. Thiophene

1. The $^2A_2$ band

The $^2A_2(\pi_3^{-1})$ photoelectron band in thiophene [Fig. 8(A)] has a rich vibrational structure of which Derrick *et al.*[4,6] identified five transitions. Additionally, one may note at least two more previously unassigned features, denoted as δ and ϵ. The Poisson intensity distribution is shown in Fig. 8(C). At this simple level of theory the experimental spectrum is quite well reproduced, allowing one to explain its

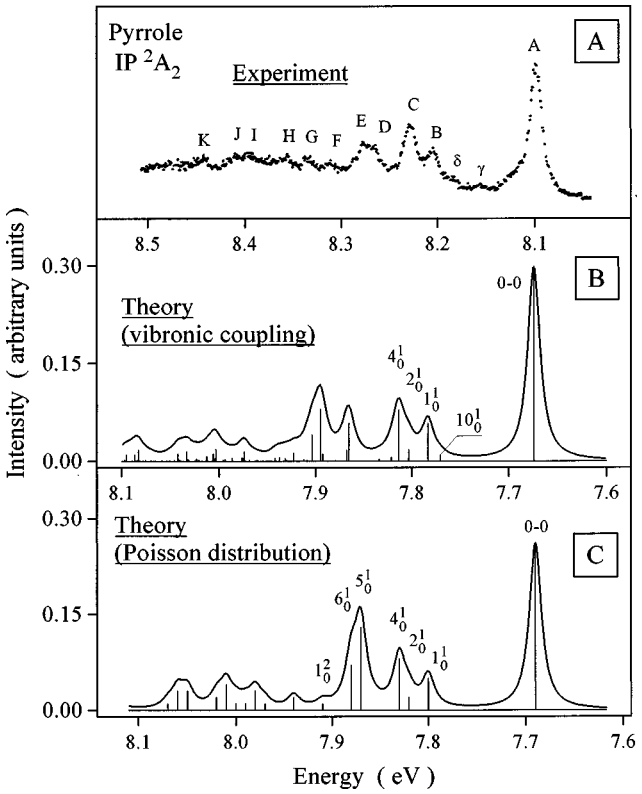

FIG. 6. Theoretical and experimental spectral envelopes of the $^2A_2(\pi_3^{-1})$ photoelectron band in pyrrole.

most important features. The computed transition frequencies also agree well with the data of Derrick *et al.*[4,6] (Table IX). The major difference between the assignments of Derrick *et al.* and ours is again only the number of active a_1 modes in the spectrum. In addition to the ν_1, ν_4 and ν_6 modes, our calculations also predict a relatively high activity of the ν_2 and ν_5 modes. Excitation of the ν_2 mode leads to the weak maximum ϵ, not assigned by Derrick *et al.* The calculations of Takeshita *et al.*[11] reproduce the main features of the experimental spectrum at low energy. However, the transition frequencies obtained in the latter work seem to be less accurate than those of our model (Table IX). The reduced frequency of the ν_1 mode in thiophene, as compared to furan and pyrrole, is probably responsible for the different shape of the thiophene $^2A_2(\pi_3^{-1})$ band.

The vibronic spectrum of the $^2A_2(\pi_3^{-1})$ photoelectron band [Fig. 8(B)] reproduces closely the spectral profile of the Poisson distribution at the low energy. The Poisson line structure is well preserved so that the features $(A-E)$ in the experimental spectrum can still be assigned to excitations of only totally symmetric vibrations. Many weaker intensity-borrowing transitions appear in the spectrum, especially at higher energy. However, except for the first one, 10_0^1, these transitions, have only little intensity and thus do not play a significant role in the spectrum. As in furan and pyrrole, the 10_0^1 transition, calculated to be 0.067 eV (540 cm^{-1}) above the 0–0 line, seems to give rise to the shoulder γ in the experimental spectrum. The calculated final-state frequency of the 10_0^1 vibration is consistent with the estimate 0.050 eV (403 cm^{-1}) obtained using Eq. (4.1). This result implies a significant reduction of the ν_{10} frequency with respect to its electronic ground state value of 769 cm^{-1}.

2. The $^2B_1$ band

The $^2B_1(\pi_2^{-1})$ photoelectron band in thiophene [Fig. 9(A)] is probably the most intriguing one among the spectra of all three molecules. The band shows no resolved structure and appears as the single broad hump with a maximum at about 9.5 eV. This shape could be reproduced only if the vibronic interaction with the $^2A_2(\pi_3^{-1})$ state is properly taken into account [Fig. 9(B)]. The effect of the interaction on the spectrum is so strong that no relation to the Poisson intensity distribution [Fig. 9(C)] can be drawn any more. At the line level, no single prominent feature can be discerned in the dense continuumlike spectrum and no assignment seems possible. The nonadiabatic effects in case of the

TABLE IX. Theoretical and experimental assignment of the vibrational structure of the $^2A_2(\pi_3^{-1})$ photoelectron band in thiophene.[a]

Experiment[b]				Poisson distribution, this work			Theory[c]		
Feature[d]	Assign.	Energy	Intens.	Assign.	Energy	Intens.[e]	Assign.[f]	Energy	Intens.
A	0	0	vs	0	0	0.19	0	0	s
δ		581	w	ν_{10}	540[g]	0.01[g]			
B	ν_1	645	s	ν_1	615	0.09	ν_1	661	s
ϵ		877	w	ν_2	870	0.01	ν_3	911	w
C	ν_4	1137	m	ν_4	1088	0.03	ν_2	1145	w
D	$2\nu_1$	1290	w	$2\nu_1$	1230	0.02	ν_4	1204	w
				ν_6	1399	0.04	$2\nu_1$	1322	w
E	ν_6	1395	s	ν_5	1464	0.14	ν_5	1459	s
				$\nu_1+\nu_2$	1485	0.01	$\nu_1+\nu_3$	1572	w

[a]See footnote a of Table VI.
[b]References 4 and 7. The data for the spectral features designated with Greek letters derived in the present work.
[c]Reference 11.
[d]See Fig. 8.
[e]See footnote e of Table VI.
[f]The final-state vibrational modes. All modes have different character in the initial and the final electronic states.
[g]See footnote g of Table VI.

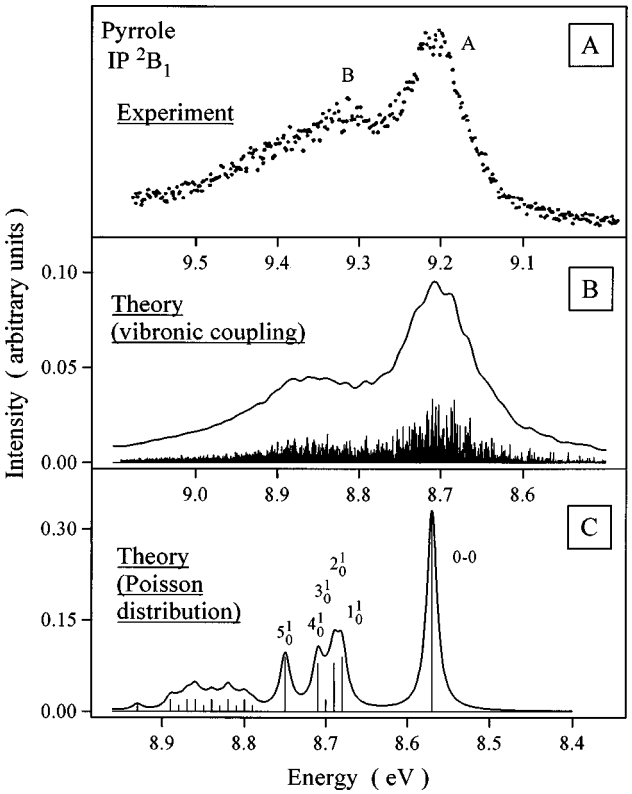

FIG. 7. Theoretical and experimental spectral envelopes of the $^2B_1(\pi_2^{-1})$ photoelectron band in pyrrole.

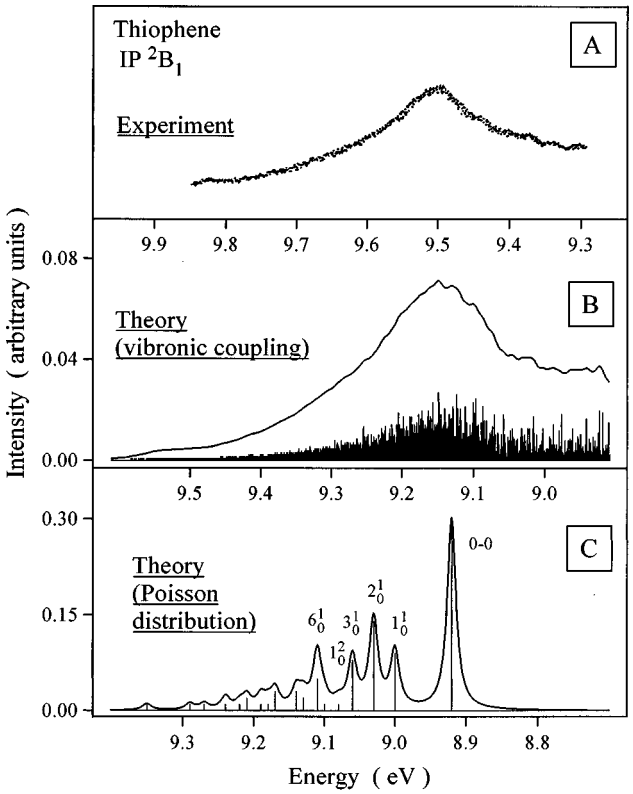

FIG. 9. Theoretical and experimental spectral envelopes of the $^2B_1(\pi_2^{-1})$ photoelectron band in thiophene.

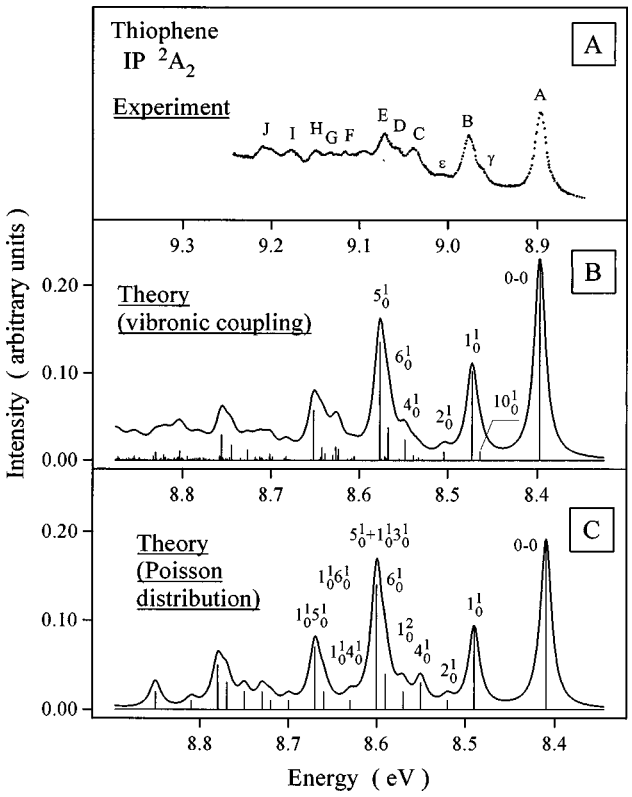

FIG. 8. Theoretical and experimental spectral envelopes of the $^2A_2(\pi_3^{-1})$ photoelectron band in thiophene.

$^2B_1(\pi_2^{-1})$ band of thiophene are strongest among the π-orbital valence-shell photoelectron spectra of all three molecules.

By contrast, the Poisson analysis predicts for the $^2B_1(\pi_2^{-1})$ band a highly structured envelope formed by an interplay of the $\nu_1-\nu_3$, ν_5 and ν_6 modes. The results reported by Takeshita *et al.*[11] are very similar to the Poisson distribution, and thus clearly irrelevant in explaining the experimental findings. These authors explain the puzzling structureless appearance of the $^2B_1(\pi_2^{-1})$ band in thiophene as follows: ''This should be connected with the fact that the tail of the first band of the $^2A_2$ state should overlap with the band of the $^2B_1$ state and the vibrational structure should not be distinguishable.'' It should be clear that a structure like that of the $^2B_1$ band cannot be the result of a simple overlapping of two vibrational progressions. The intensity of the high energy tail of the $^2A_2$ states falls off too rapidly, so that the $^2B_1$ states would not be affected to any appreciable extent.

D. Comparison of vibronic coupling in the $^2A_2$ and $^2B_1$ photoelectron bands

The results of our study have demonstrated that the coupling between the $^2A_2(\pi_3^{-1})$ and $^2B_1(\pi_2^{-1})$ states via nontotally symmetric b_2 vibrations plays an increasingly important role in the valence-shell π-ionization in the sequence of the molecules furan, pyrrole, and thiophene. The vibronic coupling depends on several factors which we will discuss in this section.

In the presence of a conical intersection between two adiabatic surfaces the nuclear dynamics can be discussed in terms of two distinct effects, referred to as ''*coupling*'' and ''*tuning*.'' [12] The *coupling* is usually regarded as the repulsion of the adiabatic surfaces $V_{1,2}$ (Sec. III B) along the coordinates of the coupling modes. The strength of the coupling along a mode ν_s is determined by the magnitude of the parameter $|\lambda_s/\omega_s|$.[12] The *tuning*, on the other hand, is related to the position of the adiabatic surfaces with respect to each other, more specifically, to the location of the seam of conical intersections and to the point of minimum energy at this seam. The energy and the coordinates of this point can be determined from the vertical energy gap E_2-E_1, the coupling constants κ_{is} and the frequencies ω_s associated with the totally symmetric modes.[12]

As follows from the λ_s values in Table IV and the frequencies of the b_2 modes in Table II, the coupling strengths are only moderate[44] in all three molecules. Consequently, the lower $(^2A_2)$ adiabatic surface does not develop a minimum at a distorted nuclear configuration, as is often the case in systems with strong coupling.[45] Another interesting observation is that the coupling strength for the three molecules is of the same magnitude. The different nonadiabatic effects in these molecules should, therefore, mainly be related to the tuning modes. Inspection of the $^2A_2$ and $^2B_1$ adiabatic surfaces shows that the conical intersection occurs at 0.51, 0.04 and 0.01 eV above the minimum of the upper $(^2B_1)$ state in furan, pyrrole, and thiophene, respectively (Table V). The lowering of the intersection point is consistent with the trend for the reduction of the vertical energy gap between the PES at the ground-state equilibrium conformation (1.47, 0.82 and 0.42 eV in furan, pyrrole and thiophene, respectively).

For a more detailed analysis, one has to take the change of the vibrational structure with the energy into account and compare the two bands separately for the three molecules. As it has been discussed in the preceding section, the lower $(^2A_2)$ band in all three molecules is well described already at the level of the Poisson distribution, and the consideration of vibronic interaction adds only some minor details. Since the conical intersection is energetically well separated from the minimum of the $^2A_2$ state, and, moreover, the coupling to the $^2B_1$ state is relatively weak, the adiabatic approximation is largely valid, that is, the spectrum of the isolated surface is a good description of the actual spectrum. This simplifies the interpretation of spectral features. The prominent transitions are clearly associated with excitations of a_1 modes. On the other hand, some weaker features that are absent in the Poisson distribution could be assigned to excitations of nontotally symmetric b_2 modes. The latter non-Franck–Condon or intensity-borrowing transitions are the signature of weak vibronic coupling between the $^2A_2$ and $^2B_1$ states.[12]

The shape of the upper $^2B_1(\pi_2^{-1})$ band changes profoundly when going from one molecule to another, but in all three cases a satisfactory theoretical description can only be obtained if vibronic interaction with the $^2A_2$ state is taken into account. In furan, the conical intersection occurs 0.51 eV above the minimum of the $^2B_1$ state. The adiabatic approximation may still be applicable for the energy region below an intersection point, and indeed, a large part of the spectrum is relatively well described by the Poisson distribution. As in the lower band, the deviation from the Poisson picture consists in the presence of additional b_2 mode excitation, which here, however, are mainly transitions associated with the lower $(^2A_2)$ surface. The mixing of the a_1 ''main'' lines of the upper $(^2B_1)$ state with the ''quasicontinuum'' of b_2 excitations leads to resonancelike structures in the $^2B_1$ spectrum. The observation of b_2 vibrations associated with the upper $(^2B_1)$ surface in the spectrum is more difficult due to the low density of such transitions in the energy region considered, which is related to the increased frequencies of the b_2 modes in the upper electronic state.

In pyrrole and thiophene the conical intersection occurs practically at the minimum of the $^2B_1$ state, and the adiabatic approximation fails for the entire $^2B_1(\pi_2^{-1})$ band. As a result of vibronic coupling, the spectra become increasingly complicated and differ completely from the Poisson distribution. The differences in the pyrrole and thiophene $^2B_1$ bands reflect some differences in the character of the coupling in these molecules. Since the coupling via individual modes is not very strong, the net effect of all b_2 modes is the important entity. (This is consistent with the observation that a satisfactory agreement with experiment required to include all b_2 modes in our calculations, except those associated with the hydrogen stretching motion.) As seen in Table IV, the number of b_2 modes with nonvanishing coupling constants λ_s in pyrrole is by one less than in thiophene. Moreover, the ν_{10} mode is expected to play a more important role in the spectrum of thiophene than of pyrrole due to the large ratio $|\lambda_s/\omega_s|$ in thiophene.

Finally we would like to mention that the remaining discrepancies between the theoretical (vibronic) and experimental spectra are probably due to inaccuracies in the parameters of the vibronic model. In the present work all parameters have been determined from *ab initio* calculations and no attempt has been made to improve these values by fitting procedures. As our experience shows, better agreement with experiment can often be achieved by slightly adjusting the vertical energy gap, the vibrational frequencies and the coupling constants.[12]

V. CONCLUDING REMARKS

In the present work we have studied the vibrational structure of the two lowest valence-shell photoelectron bands, $^2A_2(\pi_3^{-1})$ and $^2B_1(\pi_2^{-1})$, in the sequence of the heteroaromatic molecules: furan–pyrrole–thiophene. Our theoretical approach uses the results of *ab initio* modeling as the basis for subsequent treatment of the nuclear dynamics. The ground-state equilibrium geometries and vibrational frequencies have been computed at the MP2 level of theory, while the outer valence Green's functions (OVGF) method[13,30] has been employed in the calculations of the ionization energies. The cc-pVDZ basis sets[29] have been used throughout. Although the absolute accuracy of this approach with respect to vertical ionization potentials is not very high (about 0.4 eV), the relative energy and the dependence of the ionization energies on the geometric parameters are reproduced more satisfactorily. Finally, large-scale dynamic calculations treating

simultaneously two electronic states $^2A_2$ and $^2B_1$ including up to six a_1 and up to five b_2 vibrational modes have been performed within the framework of the linear vibronic coupling model.[12]

The structural similarity in the ground-state of the three molecules is preserved in the electronic structure of the ionized states. It has been found that in all three molecules the adiabatic PES of the $^2A_2(\pi_3^{-1})$ and $^2B_1(\pi_2^{-1})$ states exhibit a conical intersection at or slightly above the minimum of the upper ($^2B_1$) state. A moderately strong coupling between the two surfaces has been revealed for virtually every b_2 vibrational mode. These two effects influence the nuclear dynamics and lead to complex photoelectron bands. The lower ($^2A_2$) bands are less affected by the conical intersection, and the adiabatic approximation here holds to a good approximation. Since the coupling to the upper state is not very strong, these bands are well described already by means of the simple Poisson intensity distribution. The major spectral features could be assigned in terms of excitations of totally symmetric modes. In all molecules essentially the same set of a_1 modes (ν_1, ν_2, $\nu_4-\nu_6$) has been found to contribute to the spectra of the $^2A_2(\pi_3^{-1})$ bands. This extends the assignments of Derrick *et al.*,[4–7] who had assumed that only the ν_1, ν_4 and ν_6 modes (ν_1, $\nu_4-\nu_6$ in pyrrole) are active in this case. The present vibronic calculations clarify further details in the $^2A_2(\pi_3^{-1})$ bands. For the upper ($^2B_1$) bands, the nonadiabatic effects are much stronger and their shape could be satisfactorily reproduced only if vibronic interaction with the $^2A_2$ state is properly taken into account.

We have further analyzed the factors defining the actual structure of the observed spectra in order to establish general trends. This analysis has shown that the strength of nonadiabatic effects is mainly related to the location of the conical intersection point. The nonadiabatic effect are particularly strong in pyrrole and thiophene where the conical intersection almost approaches the bottom of the upper ($^2B_1$) state. Concomitant with the lowering of the conical intersection, there is a decrease of the vertical energy splitting between the two electronic states, $^2A_2(\pi_3^{-1})$ and $^2B_1(\pi_2^{-1})$. The differences between the spectra of pyrrole and thiophene are mainly due to the stronger net coupling in the latter case.

The results obtained in the present work demonstrate once again that the nonadiabatic effects are much more widespread and important, even in common chemical systems, than traditionally accepted. The example of the photoelectron bands of the heteroaromatic molecules furan, pyrrole and thiophene indicates that there exists a large class of chemical systems were vibronic interactions can be expected. These systems are polyatomic organic molecules of low-symmetry with well separated electronic bands which, nevertheless, can interact vibronically due to the large number of vibrational degrees of freedom. Even if the coupling via individual nontotally symmetric modes is not very strong, the net effect can become appreciable and can lead to a significant complication of the observed spectra.

ACKNOWLEDGMENTS

We thank Professor L. S. Cederbaum for his interest in this work and for valuable discussions. One of us (A.B.T.) gratefully acknowledges an Alexander von Humboldt fellowship. This work has been supported by the Deutsche Forschungsgemeinschaft and by the Russian Fund for Fundamental Research.

APPENDIX: PHOTOELECTRON INTENSITIES IN THE CASE OF VIBRONIC COUPLING

In the following we consider the dipole matrix element

$$T_m=\langle\Psi_{\epsilon m}|\hat{D}|\Psi_{00}\rangle \tag{A1}$$

taken between the initial (electronic and vibrational) ground state

$$|\Psi_{00}\rangle=|\Phi_0\rangle|\chi_{00}\rangle \tag{A2}$$

and a final state

$$|\Psi_{\epsilon m}\rangle=c_\epsilon^\dagger|\Psi_m^{N-1}\rangle \tag{A3}$$

associated with an ion in the mth vibronic state of energy e_m and a photoelectron with kinetic energy $\epsilon=h\upsilon-e_m$ ($h\upsilon$ is the photon energy). Here $\hat{D}$ denotes a component of the dipole operator, and $c_\epsilon^\dagger$ is a creation operator of second quantization for the continuum orbital $|\varphi_\epsilon\rangle$. The representation (A3) of the final state as an antisymmetrized product of the ionic state and a one-particle scattering state supposes a sufficiently high photon energy (''sudden limit'').[46,27] Moreover, we have neglected the details of the spin coupling which would lead to a factor of $\sqrt{2}$ in the spin-free final expression. In the two-state vibronic coupling problem considered in this paper the final vibronic states are represented according to Eq. (2.1) by

$$|\Psi_m^{N-1}\rangle=|\Phi_1^{N-1}\rangle|\chi_{1m}\rangle+|\Phi_2^{N-1}\rangle|\chi_{2m}\rangle, \tag{A4}$$

where $|\Phi_i\rangle$, $i=1, 2$, denote the (diabatic) electronic states corresponding to an electron vacancy in the orbital a and b, respectively. In the evaluation of Eq. (A1) one has to deal with the electronic integrals

$$D_i(\epsilon)=\langle\Phi_i^{N-1}|c_\epsilon\hat{D}|\Phi_0\rangle, \quad i=1,2, \tag{A5}$$

which, of course, may depend parametrically on the nuclear coordinates. Let us recall that in second quantization the dipole operator can be written as

$$\hat{D}=\sum_{r,s} d_{rs}c_r^\dagger c_s,$$

where $d_{rs}=\langle\varphi_r|\hat{d}|\varphi_s\rangle$ are the one-electron dipole integrals. By using

$$[c_\epsilon,\hat{D}]=\sum_s d_{\epsilon s}c_s$$

and the fact that in the sudden limit $c_\epsilon|\Phi_0\rangle=0$, the matrix elements (A5) take on the form

$$\langle\Phi_i^{N-1}|c_\epsilon\hat{D}|\Phi_0\rangle=\sum_s d_{\epsilon s}x_s^{(i)} \tag{A6}$$

where

$$x_s^{(i)}=\langle\Phi_i^{N-1}|c_s|\Phi_0\rangle \tag{A7}$$

are referred to as spectroscopic amplitudes. Under the assumption that $|\Phi_1\rangle$ and $|\Phi_2\rangle$ are well characterized as single hole states a^{-1} and b^{-1}, respectively, there is only one non-negligible spectroscopic amplitude for either state, namely, $x_a^{(1)}$ and $x_b^{(2)}$, respectively. Using these results in evaluating Eq. (A1) one obtains the following expression for the spectral function:

$$P(E)=\sum_m |T_m|^2\delta(E-e_m)$$

$$=\sum_m |d_{\epsilon a}x_a^{(1)}\langle\chi_{1m}|\chi_{00}\rangle + d_{\epsilon b}x_b^{(2)}\langle\chi_{2m}|\chi_{00}\rangle|^2\delta(E-e_m). \quad \text{(A8)}$$

In the latter equation we have used the fact that neither the dipole integrals nor the spectroscopic amplitudes depend (strongly) on the nuclear coordinates (corresponding to the Franck–Condon approximation for the diabatic states). For sufficiently high photon energy the dipole integrals do not vary much as a function of ϵ in the range of the vibronic band considered. In this limit one may also assume equal magnitudes for the two partial cross sections, that is, $|d_{\epsilon a}| \approx |d_{\epsilon b}|$. Moreover, as $|x_a^{(1)}|\approx|x_b^{(2)}|\leqslant 1$ we may put

$$x_a^{(1)}d_{\epsilon a}=x_b^{(2)}d_{\epsilon b} \quad \text{(A9)}$$

and extract these products out of the summation in Eq. (A8). Note that possible phase factors of the orbitals a and b compensate each other in the product (A9). The final result for the spectral function reads

$$P(E)=|A|^2\sum_m |\langle\chi_{1m}|\chi_{00}\rangle+\langle\chi_{2m}|\chi_{00}\rangle|^2\delta(E-e_m) \quad \text{(A10)}$$

where

$$|A|^2=|x_a^{(1)}d_{\epsilon a}|^2=|x_b^{(2)}d_{\epsilon b}|^2.$$

If, as in the present case, the electronic states belong to different symmetry species, one of the two overlap integrals $\langle\chi_{00}|\chi_{im}\rangle$, $i=1$, 2, must always vanish for symmetry reasons. Therefore, Eq. (A9) may be replaced by

$$P(E)=|A|^2\sum_m \sum_{i=1}^{2} |\langle\chi_{00}|\chi_{im}\rangle|^2\delta(E-e_m). \quad \text{(A11)}$$

In the spectral function used in Sec. II B the factor $|A|^2$ has been put to 1.

[1] *Pyrroles*, edited by R. A. Jones, E. C. Taylor, and A. Weissberger, The Chemistry of Heterocyclic Compounds, Vol. 48 (Wiley, New York, 1990/1992); *Thiophene and Its Derivatives* edited by A. Weissberger, E. C. Taylor and S. Gronowitz, The Chemistry of Heterocyclic Compounds, Vols. 3 and 44 (Wiley-Interscience, New York, 1952/1992).

[2] D. W. Turner, A. D. Baker, C. Baker, and C. R. Brundle, *Molecular Photoelectron Spectroscopy* (Wiley-Interscience, London, 1970).

[3] K. Kimura, S. Katsumata, Y. Achiba, T. Yamazaki, and S. Iwata, *Handbook of HeI Photoelectron Spectra of Fundamental Organic Molecules* (Halsted, New York, 1981).

[4] P. J. Derrick, L. Åsbrink, O. Edqvist, and E. Lindholm, Spectrochim. Acta A **27**, 2525 (1971).

[5] P. J. Derrick, L. Åsbrink, O. Edqvist, B.-Ö. Jonsson, and E. Lindholm, Int. J. Mass Spectrom. Ion Phys. **6**, 161 (1971).

[6] P. J. Derrick, L. Åsbrink, O. Edqvist, B.-Ö. Jonsson, and E. Lindholm, Int. J. Mass Spectrom. Ion Phys. **6**, 191 (1971).

[7] P. J. Derrick, L. Åsbrink, O. Edqvist, B.-Ö. Jonsson, and E. Lindholm, Int. J. Mass Spectrom. Ion Phys. **6**, 177 (1971).

[8] W. von Niessen, L. S. Cederbaum, and G. H. F. Diercksen, J. Am. Chem. Soc. **98**, 2066 (1976); G. De Alti and P. Decleva, Chem. Phys. Lett. **77**, 413 (1981); G. Bieri, L. Åsbrink, and W. von Niessen, J. Electron Spectrosc. Relat. Phenom. **27**, 129 (1982); H. Nakatsuji, O. Kitao, and T. Yonezawa, J. Chem. Phys. **83**, 723 (1985); M. H. Palmer, I. C. Walker, C. C. Ballard, and M. F. Guest, Chem. Phys. **192**, 111 (1995).

[9] K. Takeshita and Y. Yamamoto, Theor. Chim. Acta **92**, 199 (1995).

[10] K. Takeshita and Y. Yamamoto, J. Chem. Phys. **101**, 2198 (1994).

[11] K. Takeshita and Y. Yamamoto, Chem. Phys. **189**, 489 (1994).

[12] H. Köppel, W. Domcke, and L. S. Cederbaum, Adv. Chem. Phys. **57**, 59 (1984).

[13] L. S. Cederbaum, J. Phys. B **8**, 290 (1975); W. von Niessen, J. Schirmer, and L. S. Cederbaum, Comput. Phys. Rep. **1**, 57 (1984).

[14] W. Lichten, Phys. Rev. **131**, 229 (1963); Phys. Rev. **139**, A27 (1965); Phys. Rev. **164**, 131 (1967); F. T. Smith, Phys. Rev. **179**, 111 (1969); T. F. O'Malley, Adv. At. Mol. Phys. **7**, 223 (1971); T. Pacher, L. S. Cederbaum, and H. Köppel, Adv. Chem. Phys. **84**, 293 (1993).

[15] E. B. Wilson, Jr., J. C. Decius, and P. C. Cross, *Molecular Vibrations* (McGraw–Hill, New York, 1955).

[16] The dimensionless normal coordinates Q_s used in the present work are obtained from those of Wilson *et al.* (Ref. 15) by multiplying with $\sqrt{\omega_s}$ (where ω_s is the ground-state vibrational frequency for mode v_s).

[17] L. S. Cederbaum, W. Domcke, H. Köppel, and W. von Niessen, Chem. Phys. **26**, 169 (1977).

[18] H. Köppel, L. S. Cederbaum, and W. Domcke, J. Chem. Phys. **89**, 2023 (1988).

[19] R. Meiswinkel and H. Köppel, Chem. Phys. Lett. **201**, 449 (1993).

[20] L. Seidner, W. Domcke, and W. von Niessen, Chem. Phys. Lett. **205**, 117 (1993); C. Woywod, W. Domcke, A. Sobolewski, and H. J. Werner, J. Chem. Phys. **100**, 1400 (1994).

[21] A. C. Albrecht, J. Chem. Phys. **33**, 156 (1960).

[22] G. Herzberg and H. C. Longuet-Higgins, Discuss. Faraday Soc. **35**, 77 (1963).

[23] T. Carrington, Discuss. Faraday Soc. **53**, 27 (1972); Acc. Chem. Res. **7**, 20 (1974).

[24] D. R. Yarkony, Rev. Mod. Phys. **68**, 985 (1996).

[25] H. Köppel, Chem. Phys. **77**, 359 (1983); Chem. Phys. Lett. **205**, 361 (1993).

[26] W. Domcke and G. Stock, Adv. Chem. Phys. **100**, 1 (1997).

[27] J. Cullum and R. Willoughby, *Lanczos Algorithms for Large Symmetric Eigenvalue Problems* (Birkhäuser, Boston, 1985), Vols. I and II.

[28] L. S. Cederbaum and W. Domcke, Adv. Chem. Phys. **36**, 205 (1977).

[29] T. H. Dunning, Jr., J. Chem. Phys. **90**, 1007 (1989).

[30] GAUSSIAN 94, Revision C.2, M. J. Frisch, G. W. Trucks, H. B. Schlegel, P. M. W. Gill, B. G. Johnson, M. A. Robb, J. R. Cheeseman, T. Keith, G. A. Petersson, J. A. Montgomery, K. Raghavachari, M. A. Al-Laham, V. G. Zakrzewski, J. V. Ortiz, J. B. Foresman, J. Cioslowski, B. B. Stefanov, A. Nanayakkara, M. Challacombe, C. Y. Peng, P. Y. Ayala, W. Chen, M. W. Wong, J. L. Andres, E. S. Replogle, R. Gomperts, R. L. Martin, D. J. Fox, J. S. Binkley, D. J. Defrees, J. Baker, J. P. Stewart, M. Head-Gordon, C. Gonzalez, and J. A. Pople, Gaussian, Inc., Pittsburgh, PA, 1995.

[31] F. Mata, M. C. Martin, and G. O. Sörensen, J. Mol. Struct. **48**, 157 (1978).

[32] L. Nygaard, J. T. Nielsen, J. Kirchheimer, G. Maltesen, J. Rastrup-Andersen, and G. O. Sörensen, J. Mol. Struct. **3**, 491 (1969).

[33] B. Bak, D. Christensen, L. Hansen-Nygaard, and J. Rastrup-Andersen, J. Mol. Spectrosc. **7**, 58 (1961).

[34] R. C. Lord, Jr. and F. A. Miller, J. Chem. Phys. **10**, 328 (1942).

[35] D. W. Scott, J. Mol. Spectrosc. **31**, 451 (1969).

[36] D. W. Scott, J. Mol. Spectrosc. **37**, 77 (1971).

[37] M. Rico, M. Barrachina, and J. M. Orza, J. Mol. Spectrosc. **24**, 133 (1967).

[38] Results of Morcillo and Orza, as quoted in Ref. 36.

[39] R. Rico, J. M. Orza, and J. Morcillo, Spectrochim. Acta **21**, 689 (1965).

[40] The observed overall shift of the theoretical spectrum with respect to the experimental one results from an error in the calculated vertical ionization energies (Sec. III C). This kind of disagreement is disregarded in the present paper as the absolute energy values are only of a minor importance for our study of vibrational excitations. For the same reason the overall shift acquired by the spectra computed in different approximations is also not discussed in the following. The compared spectral envelopes are

aligned everywhere so as to ensure their maximal coincidence.

[41] The theoretical approach of Takeshita *et al.* (Refs. 9–11) is based on the separate description of the initial and final electronic states. It, therefore, accounts for the changes in the normal coordinates and vibrational frequencies due to ionization. In the case of simple Poisson intensity distributions the final-state vibrational frequencies are assumed to be the same as in the electronic ground state.

[42] Because our calculations are performed in the diabatic basis where the final states are described by Eqs. (2.1) and (2.6), the interpretation of the results represents a difficult task. Even when the actual physical situation is simple (e.g., when the adiabatic approximation holds) we have to resort to additional considerations to aid the assignment. A rigorous theoretical approach would be to transform the results to the adiabatic basis which is, however, not feasible for computational reasons.

[43] The estimate of the final-state vibrational frequency [Eq. (4.1)] is derived by considering a model in which two electronic states interact only via a single nontotally symmetric mode υ_s. After transforming the corresponding Hamiltonian to the adiabatic basis and neglecting the coupling between adiabatic surfaces via the kinetic energy, one obtains harmonic oscillator equations associated with each surface, containing the modified frequencies ω_s' (Ref. 12).

[44] According to the classification of Ref. 12 the coupling along υ_s is referred to as strong when $|\lambda_s/\omega_s| \gg 1$.

[45] The form of the lower adiabatic surface has been investigated within the present vibronic coupling model using relations derived in Ref. 12.

[46] T. Åberg, Phys. Rev. **156**, 35 (1967); R. L. Martin and D. A. Shirley, J. Chem. Phys. **64**, 3685 (1976).